

Singlet-triplet excitations and high-field magnetization in CuTe₂O₅

Zhe Wang, Michael Schmidt, Yurii Goncharov, Yurii Skourski, Joachim Wosnitza, Helmuth Berger, Hans-Albrecht Krug von Nidda, Alois Loidl, Joachim Deisenhofer

Angaben zur Veröffentlichung / Publication details:

Wang, Zhe, Michael Schmidt, Yurii Goncharov, Yurii Skourski, Joachim Wosnitza, Helmuth Berger, Hans-Albrecht Krug von Nidda, Alois Loidl, and Joachim Deisenhofer. 2011. "Singlet-triplet excitations and high-field magnetization in CuTe₂O₅." Journal of the Physical Society of Japan 80 (12): 124707.
<https://doi.org/10.1143/jpsj.80.124707>.

Nutzungsbedingungen / Terms of use:

licgercopyright

Dieses Dokument wird unter folgenden Bedingungen zur Verfügung gestellt: / This document is made available under these conditions:

Deutsches Urheberrecht

Weitere Informationen finden Sie unter: / For more information see:

<https://www.uni-augsburg.de/de/organisation/bibliothek/publizieren-zitieren-archivieren/publiz/>



Singlet–Triplet Excitations and High-Field Magnetization in CuTe_2O_5

Zhe WANG¹, Michael SCHMIDT¹, Yurii GONCHAROV^{1,2}, Yurii SKOURSKI³, Joachim WOSNITZA³,
Helmuth BERGER⁴, Hans-Abrecht KRUG VON NIDDA¹, Alois LOIDL¹, and Joachim DEISENHOFER¹

¹Experimental Physics V, Center for Electronic Correlations and Magnetism, Institute for Physics,
Augsburg University, D-86135 Augsburg, Germany

²General Physics Institute of the Russian Academy of Sciences, 119991 Moscow, Russia

³Hochfeld-Magnetlabor Dresden (HLD), Helmholtz-Zentrum Dresden-Rossendorf, D-01314 Dresden, Germany

⁴Institute de Physique de la Matière Complexe, EPFL, CH-1015 Lausanne, Switzerland

By measuring the THz electron spin resonance (ESR) transmission spectra and high-field magnetization on the spin-gapped system CuTe_2O_5 , we identified the singlet–triplet excitations in the dimerized non-magnetic ground state. The determined spin-gap value of $h\nu_0 = 4.94 \text{ meV}$ at the Γ point ($\mathbf{Q} \simeq \mathbf{0}$) is significantly smaller than the strongest antiferromagnetic exchange interaction between the Cu ions predicted by theoretical investigations. We also observed the critical field $H_{\text{cl}}^a = 37.6 \text{ T}$ for $\mathbf{H} \perp bc$ -plane and $H_{\text{cl}}^{bc} = 40.6 \text{ T}$ for $\mathbf{H} \parallel bc$ -plane at the onset of non-zero magnetization, consistent with the gap value and corresponding anisotropic g -factors determined previously. The observed singlet–triplet excitations in Faraday and Voigt configurations suggest a mixing of the singlet state with the $S_z = 0$ triplet state and the $S_z = \pm 1$ triplet states, respectively, due to the Dzyaloshinskii–Moriya (DM) interaction with a DM vector perpendicular to the crystalline bc -plane.

1. Introduction

During the past decades, transition-metal compounds based on Cu^{2+} ions with a $3d^9$ configuration and spin-1/2 have been intensively studied due to the observation of various exotic collective phenomena in these systems.^{1,2)} A spin gap has been observed in those systems consisting of structural Cu dimers with predominant antiferromagnetic intradimer interaction, which is crucial for the occurrence of Bose–Einstein condensation of magnons such as in TiCuCl_3 ^{3,4)} and $\text{BaCuSi}_2\text{O}_6$.⁵⁾ In another type of spin-gapped systems based on Cu dimers, CuTe_2O_5 as a particular example, the exchange interaction within the structural Cu dimer is not predominant, whereas the complex exchange paths between Cu ions mediated by the lone-pair cation of Te^{4+} were found to be even stronger.⁶⁾ Due to these complex exchange paths, it is still under debate whether the magnetic structure of CuTe_2O_5 is an alternating spin-chain (i.e., one-dimensional) or an essentially two-dimensional coupled dimer system.^{6–11)}

As shown in Fig. 1, CuTe_2O_5 exhibits a monoclinic crystal structure with space group $P2_1/c$ and lattice parameters $a = 6.817 \text{ \AA}$, $b = 9.322 \text{ \AA}$, $c = 7.602 \text{ \AA}$, and $\beta = 109.08^\circ$.¹²⁾ There are four Cu ions in one unit cell. Each Cu ion is surrounded by six oxygen atoms forming a strongly distorted octahedron. Two neighboring octahedra along the c -axis sharing an edge form structural dimer units Cu_2O_{10} , which are separated by Te–O bridging ligands. The high-temperature magnetic susceptibility of CuTe_2O_5 can be fitted by a Curie–Weiss law with a Curie–Weiss temperature of $\Theta = -41 \text{ K}$.¹⁾ At $T = 56.6 \text{ K}$ the susceptibility shows a maximum followed by a strong decrease to lower temperatures,¹⁾ which is typical for magnetic dimer systems.¹³⁾ However, the susceptibility cannot be well fitted by the model of isolated magnetic dimers.⁶⁾ Moreover, the isolated dimer model also faced difficulties in explaining the results of electron spin resonance (ESR). The extended Hückel

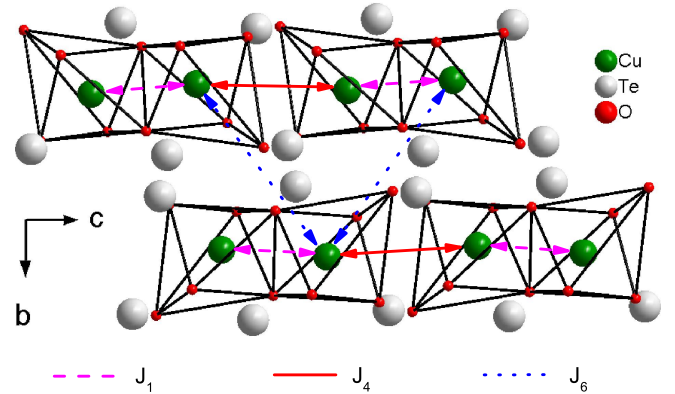


Fig. 1. (Color online) Crystal structure of CuTe_2O_5 with space group $P2_1/c$. Structural dimers consisting of edge-sharing octahedra Cu_2O_{10} are separated by Te ions. J_1 , J_4 , and J_6 are the exchange interactions between the first-, fourth-, and sixth-nearest-neighboring Cu ions, respectively.

tight-binding (EHTB) method has been used to investigate the possible exchange paths.⁶⁾ It has been shown that the exchange interaction between the sixth-nearest-neighboring Cu ions by a single O–Te–O bridge (J_6) is strongest and the nearest-neighboring interaction within the structural dimer (J_1) is the second strongest, while other exchange paths lead to much smaller exchange interactions between the Cu ions (see Fig. 1 for exchange paths). In contrast to the results of EHTB, *ab initio* density-functional theory (DFT) calculations within the local-density approximation (LDA) claimed that the strongest exchange interaction is between the fourth-nearest-neighboring Cu ions by two O–Te–O bridges (J_4 , see Fig. 1) with the second and third strongest being J_6 and J_1 , respectively,⁷⁾ indicating that CuTe_2O_5 is a two-dimensional coupled spin-dimer system. Direct computation of exchange constants by an LDA+ U approach qualitatively showed a similar result,¹⁰⁾ but determined a smaller value of

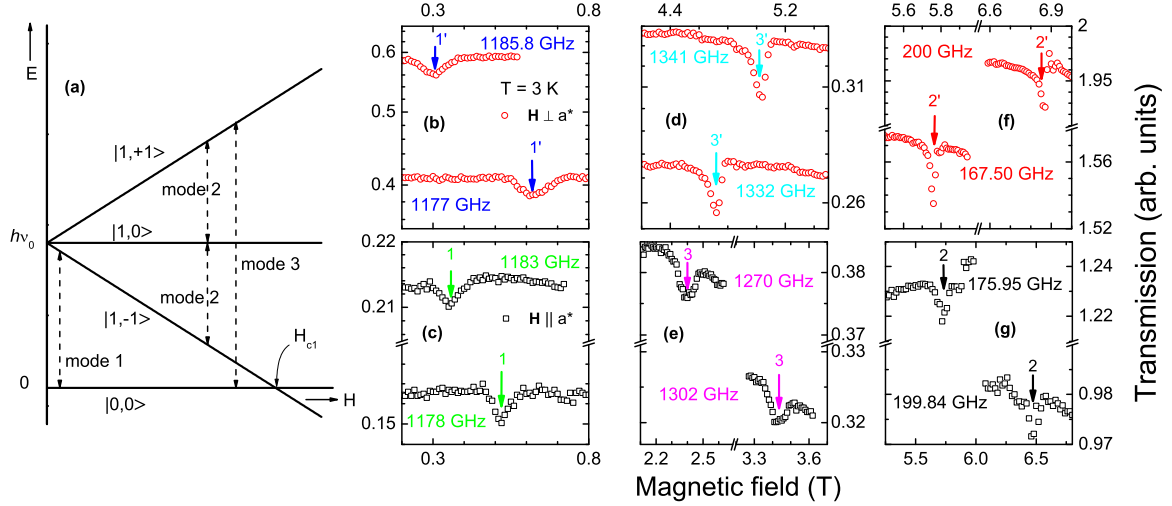


Fig. 2. (Color online) (a) Spin singlet $|0,0\rangle$ and Zeeman splitting of triplet states $|1,0\rangle$, $|1,-1\rangle$, and $|1,+1\rangle$ in a magnetic field \mathbf{H} . Modes 1 and 3 are excitations from singlet to triplet states; Modes 2 are transitions between split-triplet states. H_{c1} is explained in the text. (b)–(g) Transmission spectra measured at 3 K as a function of \mathbf{H} at various frequencies corresponding to modes 1, 3, and 2 for $\mathbf{H} \parallel a^*$, and mode 1', 3', and 2' for $\mathbf{H} \perp a^*$.

the leading exchange constant $J_4 = 5.5$ meV (~ 64 K) than the value of $J_4 = 7.96$ meV (~ 92.4 K) obtained by quantum Monte Carlo (QMC) simulations.⁷ In this paper, we report on the results of high-field ESR transmission spectroscopy up to 1.4 THz and high-field magnetization measurements up to 60 T in CuTe_2O_5 . A spin singlet-to-triplet excitation of 4.94 meV has been resolved, which is considerably smaller than the strongest exchange interaction obtained by mean-field approximation⁶ or QMC.⁷

2. Experimental Procedure

Single crystals of CuTe_2O_5 were grown by a halogen vapor transport technique, using HBr as transport agent. The charge and growth-zone temperatures were 580 and 450 °C, respectively. The stoichiometry of the single crystal was probed by electron-probe microanalysis and X-ray diffraction. THz transmission experiments were performed in the Faraday (propagating vector $\mathbf{k} \parallel \mathbf{H} \perp bc$ -plane) and Voigt configuration ($\mathbf{k} \perp \mathbf{H} \parallel bc$ -plane) using a Mach-Zehnder-type interferometer with backward-wave oscillators covering the frequency range 135 GHz–1.35 THz and a magneto-optical cryostat (Oxford/Spectromag) with applied static magnetic field \mathbf{H} up to 7 T. Magnetization measurements were performed in pulsed magnetic fields up to 60 T at the Dresden High Magnetic Field Laboratory.¹⁴

3. Results and Discussion

An isolated spin dimer with antiferromagnetic intradimer interaction exhibits a non-magnetic spin-singlet ground state and a three-fold degenerate spin-triplet excited state. In an applied magnetic field, the triplet state is completely split due to Zeeman interaction [see Fig. 2(a)], thus there are three distinct types of excitations in a spin dimer. Modes 1 and 3 correspond to excitations between the singlet state $|0,0\rangle$ and the triplet states $|1,-1\rangle$, and $|1,+1\rangle$, respectively. Mode 2 corresponds to excitations between the split triplet states $|1,-1\rangle$ and $|1,0\rangle$, or between $|1,0\rangle$ and $|1,+1\rangle$.

Figures 2(b)–2(g) shows the ESR transmission spectra as a function of magnetic field measured at different frequencies with $\mathbf{H} \parallel a^*$ or $\mathbf{H} \perp a^*$, where a^* denotes the direction

perpendicular to the bc -plane. Absorptions can be clearly observed in these spectra as marked by the arrows. The following features can be directly extracted from the data:

(i) *Energy scale.* The absorptions shown in Figs. 2(b)–2(e) are obtained at the high-frequency range ($f > 1$ THz) with relatively small field ($H < 5.2$ T). In contrast, the absorptions in Figs. 2(f) and 2(g) have much lower frequencies ($f \leq 200$ GHz) and high fields ($H > 5.6$ T). As suggested by the magnetic susceptibility and LDA+ U calculations,^{1,6,7,10} the leading antiferromagnetic interaction J_4 should not be smaller than 3.7 meV (~ 0.9 THz), while the Zeeman energy is about 0.85 meV (~ 206 GHz) at 7 T for a g -factor of 2.1.⁶ Therefore, we can distinguish mode 2 in Figs. 2(f) and 2(g) from modes 1 and 3 in Figs. 2(b)–2(e).

(ii) *Field dependence.* The resonance field shifts to larger value with higher photon frequency in Figs. 2(f) and 2(g) confirming the assignment of mode 2. A similar frequency dependence found in Figs. 2(d) and 2(e) enables us to assign the mode 3, while the reverse situation in Figs. 2(b) and 2(c) is a feature of mode 1 [see Fig. 2(a)].

(iii) *Orientation dependence.* The resonance field obtained at 200 GHz with $\mathbf{H} \perp a^*$ [Fig. 2(f)] shifts strongly away from that measured at 199.84 GHz with $\mathbf{H} \parallel a^*$ [Fig. 2(g)]. Since the frequencies are essentially the same, the large shift of resonance field with the variation of field orientation can be ascribed to the strong anisotropy of the g -factor as explained in the following. A similar feature can be observed by comparing the lines measured with different orientations of applied field in Figs. 2(b) and 2(c).

According to these features, the ESR modes can be unambiguously identified as mode 1, 2, or 3 for $\mathbf{H} \parallel a^*$, and mode 1', 2', or 3' for $\mathbf{H} \perp a^*$, as marked by the arrows in Figs. 2(b)–2(g).

The temperature-dependent behavior of the gapless intratriplet modes has been reported previously.⁶ The intensity of the gapless mode decreases exponentially with decreasing temperature below 50 K. This is a typical feature of a spin-dimer system owing to the depopulation of the spin-triplet state at lower temperatures, which is also observed in the compound based on Cr^{5+} dimers.¹⁵ Accordingly, the

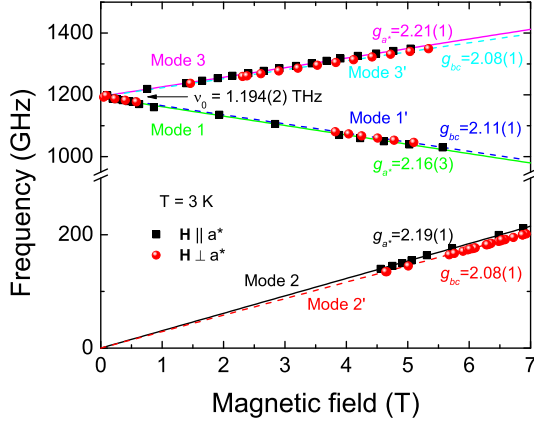


Fig. 3. (Color online) Resonance frequencies of the observed absorption lines as a function of applied magnetic field for the field parallel and perpendicular to a^* .

intensity of the gapped mode increases towards lower temperature.

The photon frequencies, at which the absorption lines were observed, are summarized as a function of the corresponding resonance fields in Fig. 3 for $\mathbf{H} \parallel a^*$ and $\mathbf{H} \perp a^*$. The observed modes differ for the two orientations of magnetic field. As intra-triplet excitations, modes 2 and 2' are fitted by lines through the origin, resulting in the effective g -factors $g_{a^*} = 2.19(1)$ and $g_{bc} = 2.08(1)$ for $\mathbf{H} \parallel a^*$ and $\mathbf{H} \perp a^*$, respectively. The g -factors are consistent with the values $g_{a^*} = 2.27(2)$, and $g_{bc} = 2.11(3)$ obtained from X- and Q-band ESR, from which a nearly constant g -factor in the bc -plane was also demonstrated.⁶⁾ Modes 1 (1') and 3 (3') can be described in terms of a linear Zeeman splitting following $h\nu = h\nu_0 \mp g\mu_B H$ with $g_{a^*} = 2.16 \pm 0.03$ ($g_{bc} = 2.11 \pm 0.01$) and $g_{a^*} = 2.21 \pm 0.01$ ($g_{bc} = 2.08 \pm 0.01$), respectively, and a coincident zero-field value of $\nu_0 = 1.194(2)$ THz (~ 4.94 meV). These g -factors, slightly larger than the spin-only value of $g = 2$, are typical for the $3d^9$ electron configuration of Cu^{2+} in distorted oxygen octahedra, where the orbital momentum is nearly quenched by the crystal field.¹⁶⁾ Both LDA and EHTB calculations have revealed that the important exchange paths in CuTe_2O_5 are lying in the layers parallel to the bc -plane, and the inter-layer exchange interactions between the Cu ions are much smaller and can be neglected. Therefore, we consider a Hamiltonian following the work by Leuenberger *et al.*¹⁷⁾ $\mathcal{H} = \sum_i J_4 \mathbf{S}_{i1} \cdot \mathbf{S}_{i2} + \sum_{(i,j')} J_6 \mathbf{S}_{i1} \cdot \mathbf{S}_{j'2} + \sum_{[i,j]} J_1 \mathbf{S}_{i1} \cdot \mathbf{S}_{j2}$, by taking into account only the three leading intra-layer interactions J_4 , J_6 , and J_1 , where i numerates the magnetic dimers (the subscripts 1 and 2 designate the two Cu ions in one dimer), (i, j') denotes the pairs of neighboring magnetic dimers correlated by J_6 , and $[i, j]$ counts the pairs of magnetic dimers correlated by J_1 (see Fig. 1). Using the standard-basis operator method within the random phase approximation,¹⁸⁾ which has been applied to study the dispersion relation in several coupled magnetic dimer systems, such as $\text{Cs}_3\text{Cr}_2\text{Br}_9$,¹⁷⁾ $\text{BaCuSi}_2\text{O}_6$,¹⁹⁾ $\text{Ba}_3\text{Cr}_2\text{O}_8$,²⁰⁾ and $\text{Sr}_3\text{Cr}_2\text{O}_8$,^{15,21)} the energy corresponding to the singlet-to-triplet excitation at the Γ point ($\mathbf{Q} \simeq \mathbf{0}$) can be approximated by $h\nu_0 \simeq \sqrt{J_4^2 + J_4\gamma}$, where $\gamma = -2J_1 + 4J_6$. According to the LDA+ U calcula-

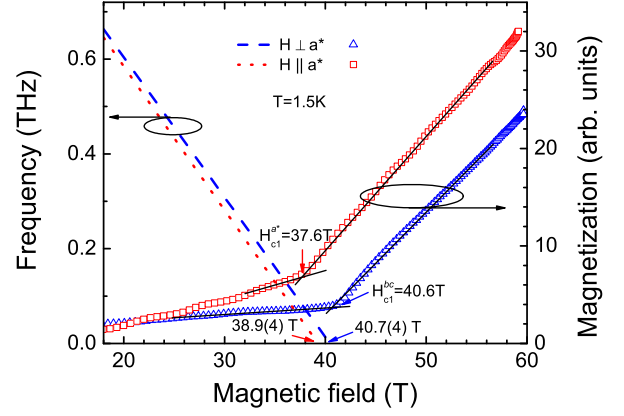


Fig. 4. (Color online) Left axis: Extrapolation of mode 1 ($\mathbf{H} \parallel a^*$, dotted line) and mode 1' ($\mathbf{H} \perp a^*$, dashed line) to the high-magnetic-field region. Right axis: Magnetization measured in a 60 T pulsed magnet at 1.5 K as a function of magnetic field for $\mathbf{H} \parallel a^*$ and for $\mathbf{H} \perp a^*$. Solid lines are guides for the eyes.

tions,¹⁰⁾ the value of $h\nu_0 = 5.32$ meV determined for $U = 10$ eV is close to the experimental result of 4.94 meV, while $h\nu_0 = 7.83$ meV is determined for $U = 8$ eV which would underestimate the on-site Coulomb repulsion in CuTe_2O_5 . It is worth noting that only the first-order perturbation of γ/J_4 is considered here, although the ratio $J_6/J_4 \sim 0.3$ given by the LDA+ U calculation is not much smaller than 1.

If there is only an isotropic intra-dimer exchange, the singlet–triplet excitation in a magnetic dimer cannot be observed in the ESR spectra. When a magnetic anisotropy via Dzyaloshinskii–Moriya (DM) interaction $\mathbf{D} \cdot (\mathbf{S}_i \times \mathbf{S}_j)$ is present, the spin-triplet states are split even in zero field.²²⁾ Moreover, the local triplet and singlet state will mix and allow the detectable optical singlet–triplet transitions.²³⁾ The singlet–triplet excitation modes 1 and 3 observed in the Faraday configuration ($\mathbf{H} \parallel a^*$) indicate a mixing of the singlet $|0, 0\rangle$ and the triplet state $|1, 0\rangle$ due to a DM vector $\mathbf{D} \parallel \mathbf{H} \parallel a^*$. For the Voigt configuration ($\mathbf{H} \perp a^*$), the DM interaction with $\mathbf{D} \parallel a^* \perp \mathbf{H}$ would mix $|0, 0\rangle$ with $|1, \pm 1\rangle$, thus the singlet–triplet excitations are also possible in this configuration, which complies with the observation of mode 1' and 3'.^{23,24)} Therefore, we conclude that the DM vector is perpendicular to the crystalline bc -plane.

As illustrated in Fig. 2(a), the Zeeman splitting will drive the lower-lying triplet state $|1, -1\rangle$ towards the singlet state and merge into the the ground state, when the magnetic field is sufficiently large and exceeds a critical field $H_{c1} = h\nu_0/g\mu_B$, with the Bohr magneton μ_B and the corresponding g -factor. At $H = H_{c1}$, a transition from a non-magnetic ground state to one with a finite magnetization is induced by the field. The finite bulk magnetization should be observed and increase with increasing field $H > H_{c1}$ due to the larger population of the lower-lying triplet state. Figure 4 shows the magnetization on the right ordinate as a function of magnetic field up to 60 T. A clear increase of magnetization can be observed at $H_{c1}^{a^*} = 37.6$ T for $\mathbf{H} \parallel a^*$ and at $H_{c1}^{bc} = 40.6$ T for $\mathbf{H} \perp a^*$, which agree with the values of 38.9(4) T and 40.7(4) T determined by $H_{c1} = h\nu_0/g\mu_B$ from mode 1 and 1' with g_{a^*} and g_{bc} , respectively, shown on the left ordinate. This confirms the spin gap of $h\nu_0 = 4.94$ meV independently by means of high-field magnetization measurements.

4. Conclusions

In summary, the magnetic properties of the spin-gapped system CuTe_2O_5 have been studied by THz electron spin resonance transmission spectroscopy and high-field magnetization measurements. The excitations from singlet to Zeeman split-triplet states and the excitations between the split-triplet states have been observed, thus a spin-gap value of $h\nu_0 = 4.94$ meV is determined. A magnetic-field-induced transition from a non-magnetic to a finite magnetization state is observed at a critical field $H_{c1}^{a^*} = 37.6$ T for $\mathbf{H} \parallel a^*$ and at $H_{c1}^{bc} = 40.6$ T for $\mathbf{H} \perp a^*$ consistent with the anisotropic g -factors and spin gap $h\nu_0$ determined from ESR spectra.

Acknowledgments

We thank M. V. Eremin of Kazan Federal University and Yuan Wan of Johns Hopkins University for fruitful discussions. We acknowledge the partial support by the DFG via TRR 80 (Augsburg-Munich) and FOR 960 (Quantum Phase Transitions). Part of this work has been supported by EuroMagNET II under the EU contract 228043.

- 1) P. Lemmens, G. Güntherodt, and C. Gros: *Phys. Rep.* **375** (2003) 1.
- 2) T. Giamarchi, C. Rüegg, and O. Tchernyshyov: *Nat. Phys.* **4** (2008) 198.
- 3) T. Nikuni, M. Oshikawa, A. Oosawa, and H. Tanaka: *Phys. Rev. Lett.* **84** (2000) 5868.
- 4) H. Tanaka, A. Oosawa, T. Kato, H. Uekusa, Y. Ohashi, K. Kakurai, and A. Hoser: *J. Phys. Soc. Jpn.* **70** (2001) 939.
- 5) M. Jaime, V. F. Correa, N. Harrison, C. D. Batista, N. Kawashima, Y. Kazuma, G. A. Jorge, R. Stern, I. Heinmaa, S. A. Zvyagin, Y. Sasago, and K. Uchinokura: *Phys. Rev. Lett.* **93** (2004) 087203.
- 6) J. Deisenhofer, R. M. Eremina, A. Pimenov, T. Gavrilova, H. Berger, M. Johnsson, P. Lemmens, H.-A. Krug von Nidda, A. Loidl, K.-S. Lee, and M.-H. Whangbo: *Phys. Rev. B* **74** (2006) 174421.
- 7) H. Das, T. Saha-Dasgupta, C. Gros, and R. Valentí: *Phys. Rev. B* **77** (2008) 224437.
- 8) R. M. Eremina, T. P. Gavrilova, N.-A. Krug von Nidda, A. Pimenov, J. Deisenhofer, and A. Loidl: *Phys. Solid State* **50** (2008) 283.
- 9) T. P. Gavrilova, R. M. Eremina, H.-A. Krug von Nidda, J. Deisenhofer, and A. Loidl: *J. Optoelectron. Adv. Mater.* **10** (2008) 1655.
- 10) A. V. Ushakov and S. V. Streltsov: *J. Phys.: Condens. Matter* **21** (2009) 305501.
- 11) R. M. Eremina, T. P. Gavrilova, A. Günther, Z. Wang, R. Lortz, M. Johnsson, H. Berger, H.-A. Krug von Nidda, J. Deisenhofer, and A. Loidl: to be published in *Eur. Phys. J. B* [DOI: 10.1140/epjb/e2011-20263-2].
- 12) K. Hanke, V. Kupcik, and O. Lindqvist: *Acta Crystallogr., Sect. B* **29** (1973) 963.
- 13) B. Bleaney and K. D. Bowers: *Proc. R. Soc. London, Ser. A* **214** (1952) 451.
- 14) J. Wosnitzer, A. D. Bianchi, J. Freudenberger, J. Haase, T. Herrmannsdörfer, N. Kozlova, L. Schultz, Y. Skourski, S. Zherlitsyn, and S. A. Zvyagin: *J. Magn. Magn. Mater.* **310** (2007) 2728.
- 15) Z. Wang, M. Schmidt, A. Günther, S. Schaile, N. Pascher, F. Mayr, Y. Goncharov, D. L. Quintero-Castro, A. T. M. N. Islam, B. Lake, H.-A. Krug von Nidda, A. Loidl, and J. Deisenhofer: *Phys. Rev. B* **83** (2011) 201102.
- 16) A. Abragam and B. Bleaney: *Electron Paramagnetic Resonance of Transition Ions* (Clarendon Press, Oxford, U.K., 1970) p. 455.
- 17) B. Leuenberger, A. Stebler, H. U. Güdel, A. Furrer, R. Feile, and J. K. Kjems: *Phys. Rev. B* **30** (1984) 6300.
- 18) S. B. Haley and P. Erdős: *Phys. Rev. B* **5** (1972) 1106.
- 19) Y. Sasago, K. Uchinokura, A. Zheludev, and G. Shirane: *Phys. Rev. B* **55** (1997) 8357.
- 20) M. Kofu, J. H. Kim, S. Ji, S. H. Lee, H. Ueda, Y. Qiu, H. J. Kang, M. A. Green, and Y. Ueda: *Phys. Rev. Lett.* **102** (2009) 037206.
- 21) D. L. Quintero-Castro, B. Lake, E. M. Wheeler, A. T. M. N. Islam, T. Guidi, K. C. Rule, Z. Izaola, M. Russina, K. Kiefer, and Y. Skourski: *Phys. Rev. B* **81** (2010) 014415.
- 22) T. Sakai, O. Cépas, and T. Ziman: *J. Phys. Soc. Jpn.* **69** (2000) 3521; T. Sakai, O. Cépas, and T. Ziman: *Physica B* **294–295** (2001) 26.
- 23) T. Rööm, D. Hüvonen, U. Nagel, Y.-J. Wang, and R. K. Kremer: *Phys. Rev. B* **69** (2004) 144410.
- 24) M. Matsumoto, T. Shoji, and M. Koga: *J. Phys. Soc. Jpn.* **77** (2008) 074712.